Preliminary results of the 40 m radiotelescope at 88 GHz

P. de Vicente, R. Bolaño, J. A. López Fernández
J. A. López Pérez, F. Tercero

Informe Técnico IT-OAN 2010-16

Revision history

Version	Date	Author	Updates
1.0	05-02-2010	P. de Vicente	Draft
1.1	15-11-2010	P. de Vicente	Completed, reviewed and corrected

Contents

1 Introduction

This report describes the first results obtained with the 3 mm receiver installed in the 40 m radiotelescope. This receiver was delivered by IRAM and operated previously in the Plateu de Bure interferometer. A new optical system was built to include the 3 mm receiver in the 40 m mirror optical system at the Nasmyth cabin. In order to inject the frontend signal into the VLBI system a new IF was designed and built.

The measurements performed with the 3 mm receiver were part of the software developement process (3 mm control and data acquisition and postprocessing), and hardware checking. In fact some small software bugs popped up because the system is taken to the limit at this frequency of observation. Almost all of them were solved. Occupancy of the telescope, bad weather, bug discovery and repair and the requirement of liquid helium to cool down the receiver prevented a systematic campaign to fully characterize the telescope. Therefore this report may seem incomplete to the reader but it has no other aim than recording the first results at 3 mm and estimating the main parameters of the telescope at this wavelength before the adjustement of the antenna surface with holography which started in August 2010.

2 Receiver-Backend setup description

The 87 GHz receiver was installed at the 40m radiotelescope in December 2009 and the first radio detection performed by the 40 m radiotelescope was obtained in December 11th 2009. Fig. 1 shows a picture of the receiver. The IF was built from scratch at the OAN labs in Yebes and details are described by Cordobés et al (2009).

The 40m radiotelescope is a Nasmyth antenna and the radiation detected at the 87 GHz receiver reflects on 9 mirrors before arriving at the horn. As with all receivers in the VLBI branch, radiation is reflected on M1 (the main reflector), M2 (subreflector), M3 (planar rotating mirror) and M4' (planar mirror). Then radiation goes through the central hole of the parabola and reflects on M22 (an offset elliptic), on two elliptical mirrors (M6 and M7), a planar mirror with a grid to separate polarizations, and a final elliptic mirror. In order to align the receiver, all mirrors after M22 were grooved with a grid that allowed to see a red laser.

The 87 GHz receiver has a single linear polarization, but circular polarization is possible inserting a quarter wavelength plate between elliptical mirrors M6 and M7. An Agilent synthesizer with a multiplying head acts as local oscillator. The instantaneous bandwidth is 625 MHz. The receiver is double side band with a possible maximum 20 dB rejection in the image band. The rejection level depends on the frequency of observation. The receiver can see a hot load, and a cold load inside the cryostat. The hot load is at environment temperature (usually 293 K) and the cold load at 15.6 K. Loads are remotely controlled and integrated in the overall control system of the receiver. Inserting and removing the load takes 1 second at most.

The IF signal is converted to a 500-1000 MHz band and sent to the backends room where it is injected in the VLBA terminal and from there connected to a spectral or a continuum backend.

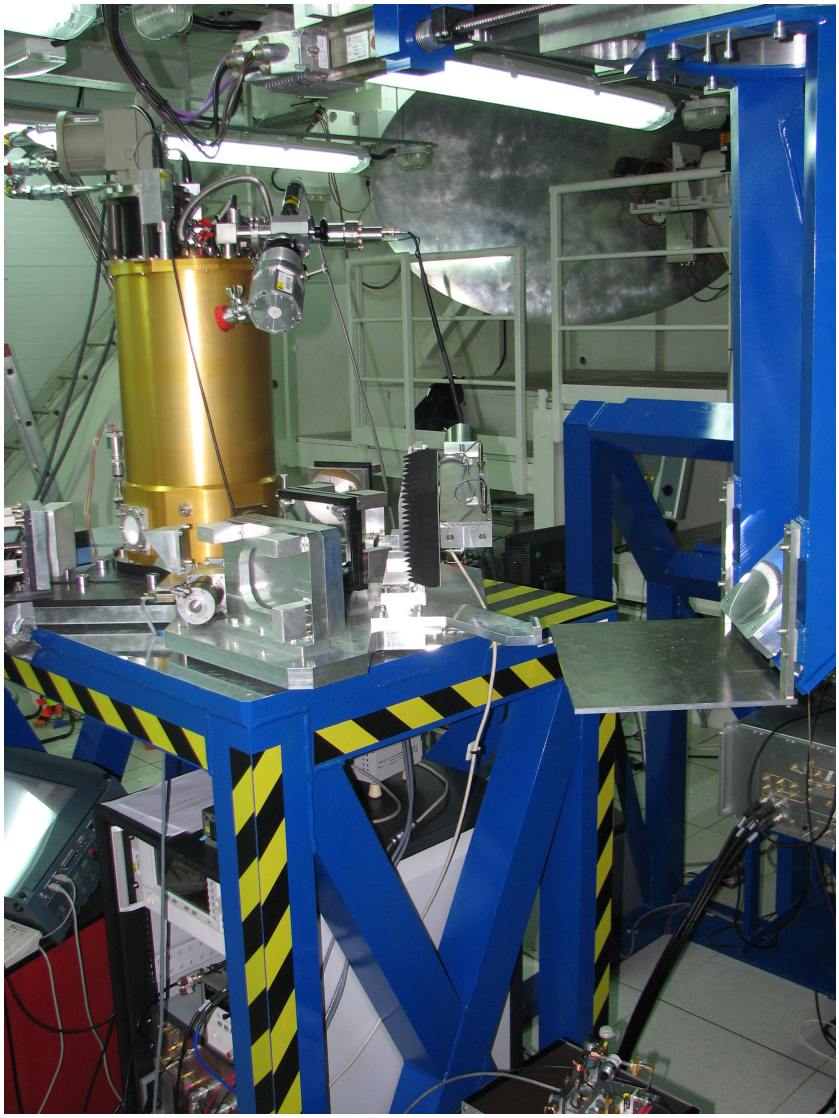

Figure 1: *3 mm receiver at the receiver cabin*

3 First observations: software and telescope issues

The first detection was obtained in December 11th towards Saturn making a pointing drift. Observations were resumed in February 2010 and lasted for some months in a very discontinued way. Only four sources are bright enough to be detected, Mars, Jupiter, Saturn and Venus. Fig. 2 contains a drift on Venus and Saturn. Efforts to detect 3C454.3 (28 Jy), 3C274 ($>$ 10 Jy) and DR21 ($>$ 10 Jy) were unsuccessful.

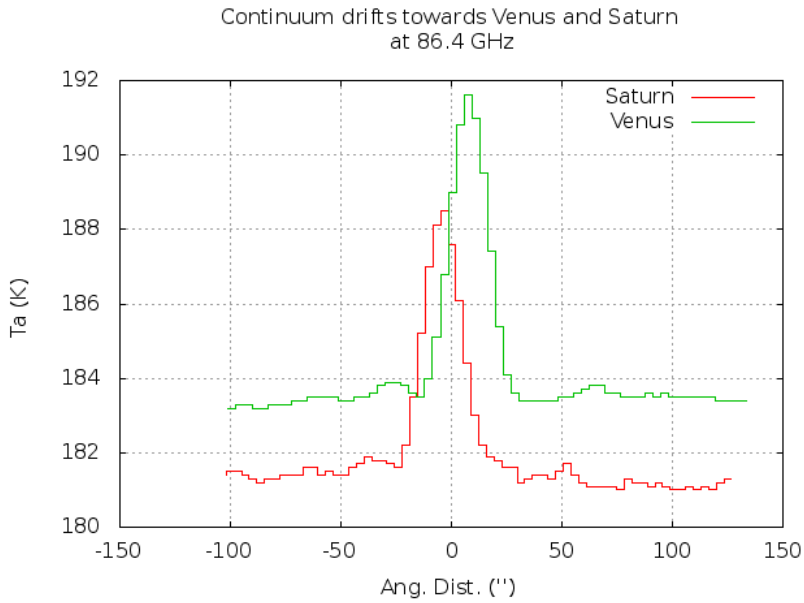

Figure 2: *Continuum drift in azimuth towards Venus and Saturn at 86.4 GHz*

Pointing drifts on planets at 3 mm discovered a number of problems which we list below.

- Planet positions were not accurately computed and hence source tracking and offsets from pointing drifts were not correct. The position of planets was computed only once, everytime the source was commanded from the ARIES command line. This behaviour was changed and now the position of any planet is computed at the beginning of each scan. Recorded data contain offsets between the current telescope position and the expected source position. The latter is computed immediately before a data is acquired and immediately after it. The mean value is obtained and associated with the data acquired.

- Under some circumstances the time in the antenna control computers was incorrect, even if the NTP daemon was apparently active. We solved this issue, and currently, everytime an observer starts the ARIES command line, the time is checked against the OAN stratum 0 NTP server and the information logged on the screen. If there is an error it will be easily noticeable by the operator.

- Sometimes, scans aborted spontaneously after some time. This was caused by a deep bug in the software that reads and writes scan information in the database. The error was trig-

gered by the great number of observations performed by the 40 m, around 18000 by the time the observations were done, and was not particulary related to 3 mm observations. This was corrected.

- Synthesizers pose some problems after being commanded too frequently to correct for Doppler shift due to the rotation of Earth. Software was modified and now frequency corrections are commanded only when the frequency change is higher than the resolution of the backend. Continuum observations do not require continuous Doppler corrections, and are only applied at the beginning of each scan.

- Remote positioning of hot and cold loads showed an unstable behaviour. We believe that this may be related to some issues with the serial port used by the IF. Some software corrections were applied and the status improved, but this issue is not completely solved yet.

- The hysteresis problem (de Vicente et al 2010a) prevented systematic pointing drifts without human intervention. These type of observations are very important to obtain data for pointing and focus models. The temporal solution was to use only encoder 1 and it was set in such a way that even after an ACU reboot only that encoder should be active. This solution reduces the hysteresis but does not solve it. Pointing errors up to 14 arcsecs may still be present. This value is very high compared to the beam size, 18 arcsecs.

- A better pointing model for 22 GHz was searched and used as input for the 3 mm one. It was not possible to obtain a 3 mm model because the low sensitivity of the antenna prevents having enough detectable sources to provide a good sky coverage.

Diagnosing and solving all these issues took time and delayed the characterization of the telescope. Results presented in this report were obtained after creating and applying solutions. Unfortunately the lack of telescope time and good weather prevented a complete characterization.

4 Receiver and system temperature

Receiver temperature is easily obtained by placing a hot and a cold load in front of the horn. Let T_r be the receiver temperature, T_h and T_c the temperature of the hot and cold loads respectively, V_h and V_c the voltages measured on the hot and cold load and V_0 the offset of the continuum detector, then:

$$T_r = \frac{T_h(V_c - V_0) - T_c(V_h - V_0)}{V_h - V_c} \tag{1}$$

Although the receiver has a continuum detector, we used the OAY-14 continuum detector connected to the IF. The IF signal, as with the rest of receivers, is cabled to one of the 4 IF inputs of the VLBI terminal. In this way we can obtain the offset of the continuum detector by attenuating the signal 20 dB and using the external IF input from the VLBI terminal.

Receiver temperature at 3 mm depends critically on mixer tuning for each frequency and on the side band mode: either single side band or double side band. Receiver temperature can be as low as 40 K at 88.4 GHz and if the mixer is incorrectly tuned, up to 120 K.

System temperatures depend strongly on the atmosphere and vary from 190 K in single side band to 340 K or higher under bad weather conditions.

5 Skydips and opacity

Skydips presented here were done in February and March 2010. Fig. 3 shows six curves with a variety of atmospheric conditions that demonstrate that the water content in the atmosphere plays a very important role in the opacity at 3 mm. All of them show an odd behaviour at elevations larger than 65 degrees. The curve between 65 and 90 degrees should stay flat or decrease slowly. However we see an increase, abrupt in some cases, as elevation increases. We believe that this behaviour comes from the membrane at the vertex which is tilted 65 degrees with respect to the walls of the vertex tube to force the water drop when it is at stow position (90 degrees elevation). When the antenna is pointing towards the zenith the membrane forms an angle of 30 degrees with the horizon, whereas it forms an angle of 0 degrees (it is parallel to the ground) when elevation is 65 degrees. When the antenna looks towards the horizon, the membrane is upside down and forms 65 degrees with the ground. Winter in 2010 was very wet and this caused the membrane to have some water on top of it. We believe that when the antenna elevation was 65 degrees the water spread all over the surface of the membrane, increasing abruptly the system temperature.

The antenna temperature of the sky (T^a_{sky}) can be written as below:

$$T^a_{sky} = \eta_f T_{atm}(1 - e^{-\tau_0 A}) + T_{rx} + T_g(1 - \eta_f) \quad (2)$$

where η_f is the forward eficciency and represents the fraction of radiation that enters the horn from the front part of the antenna. T_{atm} is the atmospheric temperature and, as an approximation, can be considered to be the ground temperature minus 40 degrees. τ_0 is the atmospheric opacity in the zenith and A the number of airmasses (1 towards the zenith). T_{rx} is the receiver temperature and T_g the ground temperature.

Fits to obtain forward efficiency and opacity were performed assuming that all curves should remain flat for elevations greater or equal than 65 degrees. Table 1 summarizes the values used for each curve plus the estimated opacity from ATM. Precipitable water content was obtained, as explained in de Vicente 2010b, from the dew temperature (T_d) and weather parameters in the environment of the observatory.

Dew temperature is obtained from:

$$T_d = (hr/100)^{1/8}\,(110 + T) - 110$$

where hr is the relative humidity and T the local temperature in degrees celsius. That is, $T_s = T + 273.16$

The column of precipitable water vapour depends on a scale factor in meters for the water vapour presence in the atmosphere, the relative humidity and the surface atmospheric tempera-

ture. The chosen scale factor was 2500 m.

$$h = \frac{e^{1.81+17.27\,Td/(Td+237.3)} m_{H2O}}{\rho_l\, K\, T_s}\, H$$

where ρ_l is the density of liquid water, K the Boltzman constant, m_{H2O} the mass of a molecule of water, T_s the environment temperature in Kelvin and H the scale factor.

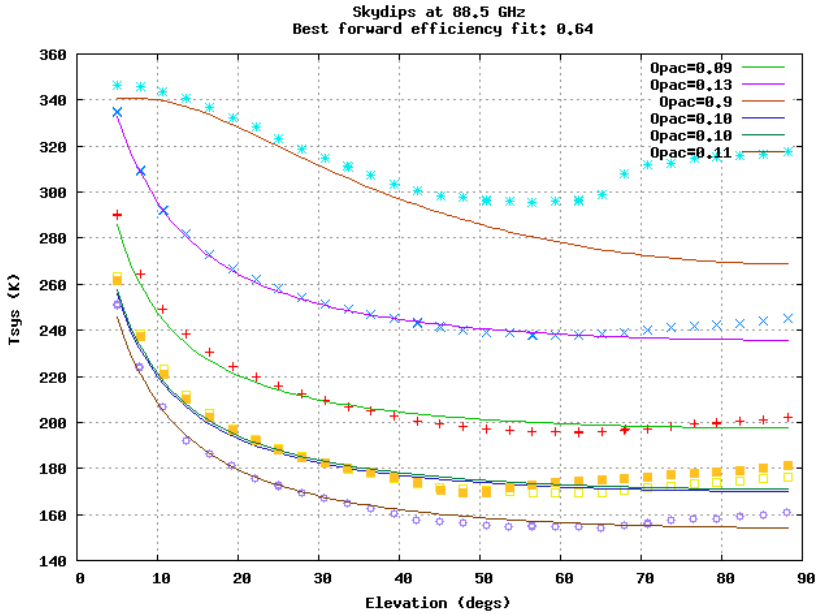

Figure 3: *Skydips at 88.4, 86.8 and 86.2 GHz. Curves have been fitted taking into account the receiver temperature and weather conditions for each case. Free parameters were opacity for each case and the same forward efficiency for all cases. The curve with the highest value is a special case since we believe that it was raining or the vertex was wet. The fit has been performed assuming that the atmosphere temperature was the same as the environment temperature since opacity was very high*

Free parameters in the fit were opacity (different for each case) and a single forward efficiency for all cases. Table 1 also includes opacity from the skydips to compare it with the estimated ones. The best fit for the forward efficiency is 0.64.

6 Aperture Efficency and main beam efficiency

Apperture efficiency (η_a) may be computed from the flux and the antenna temperature of a radiosource. According to Baars (2007):

$$\eta_a = \frac{2K_B C_s T'_a}{AS_f} \tag{3}$$

where T_a is the antenna temperature in space (no absorption from the atmosphere), A the radiotelescope collecting area, S_f the source flux and C_s a factor which takes into account the

Frequency (MHz)	η_f	τ_0 (meas.)	T_d (C)	H_2O (mm)	τ_0 (ATM)	T_{rec} (K)	Temp (C)	Hum. (%)
88450	0.64	0.09	-13.0	4.2	0.06	81	13	15
88450	0.64	0.13	-4.7	8.6	0.10	120	-1.7	80
88450	0.64	0.90	4.4	16.8	0.17	63	5.0	96
88450	0.64	0.10	-10.5	5.6	0.07	60	-5.9	70
88450	0.64	0.10	-10.6	5.4	0.07	60	-3.6	58
88450	0.64	0.11	-8.0	6.6	0.08	41	-1.3	60

Table 1: *Forward eficciency and zenital opacity, columns 2 and 3 respectively, obtained from skydips. Dew temperature, water content in the atmosphere, estimated opacity from ATM, receiver temperature (RCP), temperature and humidity are included. ATM opacity was computed from a general model for winter at Yebes and the estimated water content in mm.*

source brightness distribution compared to the antenna HPBW and is only valid for sources whose size is equal or smaller than the beam width:

$$C_s = \begin{cases} 1 + x^2 & \text{gaussian source} \\ \frac{x^2}{1-\exp(-x^2)} & \text{disk source} \end{cases} \tag{4}$$

where,

$$x = \frac{\theta_s('')}{\theta_b('')} \tag{5}$$

and θ_s is the source size and θ_b the HPBW of the antenna.

Making numbers we get:

$$\eta_a = 2.197 \frac{C_s\, T_a[\mathrm{K}] e^{\tau}}{S_f[\mathrm{Jy}]} \tag{6}$$

The aperture efficiency of the radiotelescope at 3 mm was obtained from observations towards Venus and Saturn and it is around 11%. Jupiter observations were discarded since its size is higher than the beamwidth and approximations above are not valid. The flux for Venus and Saturn was estimated using application Astro from IRAM GILDAS package. Table 2 summarizes the data, intermediate values and results.

The beam efficiency is the fraction of all power received which enters the main beam. The main beam is defined to extend to the first null in the radiation pattern. It can be computed for point like sources (Baars 2007) from:

$$\eta_{mb} = \frac{\Omega_m A_g}{\lambda^2} \eta_a \tag{7}$$

$$= \frac{\pi D^2}{4} \frac{1.133}{\lambda^2} \left(\frac{1.16\lambda}{D} \right)^2 = 0.89\, 1.16^2\, \eta_a \tag{8}$$

$$= 1.1976\, \eta_a \tag{9}$$

where Ω_m is beam solid angle, A_g the geometrical area, λ the observing length and D the diameter of the antenna. If the aperture efficiency is 11%, the main beam efficiency is approximately 13%.

Source	Size (")	Flux (Jy)	T_b (K)	T_a (K)	El (°)	τ_0	C_s	S/T_a (Jy/K)	η_a	η_{mb}
Venus	$11'' \times 11''$	196	365	8.2	41	0.20	1.135	19.3 Jy/K	0.114	0.136
Saturn	$19'' \times 17''$	204	150	7.1	37	0.16	1.387	18.7 Jy/K	0.117	0.140

Table 2: *Size, flux, brightness temperature, antenna temperature, elevation, opacity, source correction, flux antenna temperature ratio, aperture efficiency and main beam efficiency for Venus and Saturn at 86.6 GHz.*

7 Gain curve

Fig. 4 displays the gain curve obtained tracking Venus and Saturn. The data do not have good quality and hence results should be taken with great caution. Focus and pointing changed while tracking the sources. Focus changed due to the night and day temperature difference and solar illumination, and the pointing was severely affected by the encoder hysteresis (de Vicente et al 2010a). These effects are responsible of the high data dispersion. The gain curve may be approximated by fitting a function to the highest values, but in any case this should be considered as a very rough approximation. The maximum aperture efficiency is 0.11 at 40 degrees elevation.

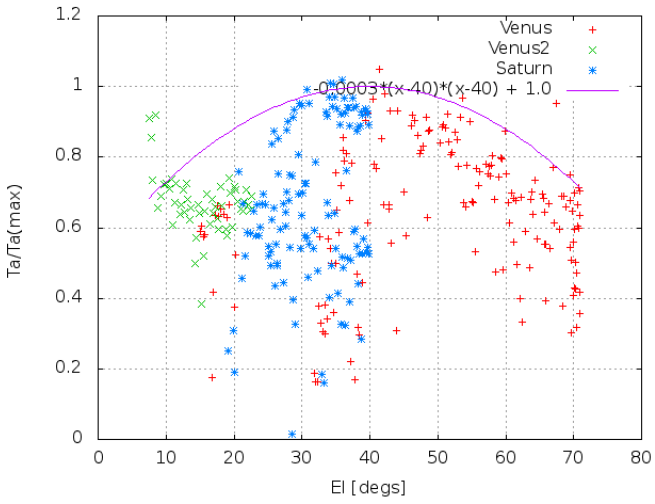

Figure 4: *Normalized antenna temperature versus elevation corrected for atmospheric opacity. The dispersion in the graph comes mainly from pointing errors*

8 Estimation of the error budget in the surface of the main reflector

The aperture efficiency depends on the blockage by the legs and the subreflector (η_b), absorption by the membrane at the vertex (η_m), surface errors in the subreflector (η_{m2}) and nasmyth mirrors (η_{nm}), and illumination eficciency (η_i). So we can summarize them as:

$$\eta_a = \eta_{m1}\eta_{m2}\eta_{nm}\eta_{block}\eta_m\eta_i \quad (10)$$

$$= \eta_{m1}\eta_{m2}\eta_{m3}\eta_{m4}\eta_{m22}\eta_{block}\eta_m\eta_i = \eta_{m1}\eta_x \quad (11)$$

where we have ignored the errors coming from all mirrors after M22.

The main reflector surface error budget may be estimated from the aperture efficiency and the rest of factors that do not come from the main reflector.

According to Malo et al. (2010), the membrane in the vertex presents a maximum loss of 1.24 dB ($\simeq$ 25%) at 100 GHz. Tercero & Finn (2010) estimate that the loss depends on the relative orientation of the membrane with respect to the horn and on the polarization. For a membrane which forms an angle of 25 degrees with the horn the loss varies between 1.3 dB (25%) and 2.3 dB (42%) approximately.

We have estimated the rms of the surface for the different mirrors, using Ruze's (1966) formula:

$$\eta_m = e^{-\frac{4\pi\sigma}{\lambda}^2} \quad (12)$$

where $\lambda = 3.3$ mm, and σ is 50 μm for the subreflector, 25 μm for M3 and M4 and 80 μm for M22.

Hence:

$$\eta_a = \eta_{m1}\, 0.967\, 0.99\, 0.99\, 0.916\, 0.92\ 0.70\eta_m = 0.60\, \eta_{m1}\, \eta_m \quad (13)$$

where the efficiency due to illumination is 0.70 (Tercero private communication).

Therefore, if we assume an interval between 11% and 38% of loss which corresponds to $\eta_m = 0.89$ and $\eta_m = 0.62$ respectively:

$$\eta_{m1} = \frac{\eta_a}{0.60\,\eta_m} = \frac{0.183}{\eta_m} \quad (14)$$

$$= 0.31\,[\eta_m = 0.58] \quad (15)$$

$$= 0.24\,[\eta_m = 0.75] \quad (16)$$

The error budget for M1 is then:

$$\sigma = \frac{\sqrt{-\ln\eta_{m1}}}{4\pi}\lambda\,[\mu\mathrm{m}] \quad (17)$$

$$\sim 298\,\mu\mathrm{m}\,[[\eta_m = 0.58] \quad (18)$$

$$\sim 329\,\mu\mathrm{m}\,[[\eta_m = 0.75] \quad (19)$$

Possible improvements may come from replacing M5 by a mirror with a $\sigma = 50\,\mu$m. This would increase the aperture efficiency by 5%. Replacing the membrane by a new one with losses of 10% would improve the efficiency 50% (if $\eta_m = 0.58$) or 20% (if $\eta_m = 0.75$). However, the most important improvement would come from the adjustement of the main reflector surface. For example, if we achieved a $\sigma = 150\,\mu$m, the aperture efficiency would be $\eta_a = 0.44$, without correcting for the membrane loss.

9 First single dish spectrum

On April 27th we obtained the first spectrum using the autocorrelator towards IKTau. The receiver was tuned at 86200 MHz close to the SiO V1 transition, 86243.430 MHz. The number of channels used were 2048 and the spectral resolution was 125 KHz per channel (0.43 km/s). Integration time was 60 seconds. Fig. 5 shows the spectrum obtained with the 40m.

In order to check the result we requested IRAM to observe the same line and source with the 30 m telescope. Fig. 6 shows the spectrum. Amplitude is in K, and to obtain the flux in Jansky it should be multiplied by 6. The observation was in polarimetry mode and as such appears in the plot.

Assuming a system temperature of 200 K for the spectrum and that the rms of the baseline is dominated by thermal noise we can calibrate approximately the spectrum. The expected sigma that we should obtain is:

$$\sigma = \frac{T_{sys}}{\sqrt{\Delta B\, T}} = 0.0730 \text{ K} \tag{20}$$

The rms of the spectrum amplitude is 138 in the arbitrary units diplayed in Fig. 5. Hence, if we consider the rms to be 3σ, the spectrum should be divided by $138/0.21 \simeq 630$ to obtain it in K and the result multiplied by 19 to obtain it in Jy. The estimated flux with the 40 m towards IK Tau is 320 Jy, which compared to 600 Jy from the 30 m, indicates that the 40 m has approximately half the sensitivity of the 30 m despite the area being 1.8 times greater. We can conclude that the aperture efficiency for the 40 m is at least 4 times lower (15%) than that of the 30 m (63%).

10 First VLBI detection

On April 21st 2010, we took part for the first time in a 2 hour fringe test at 86 GHz together with Onsala 20 m and Metsähovi 14 m telescopes. The selected source was 3C454. Data were recorded on the 3 telescopes in disk packs and later transfered to Bonn correlator using the tsunami protocol. The data in Yebes were extracted from the Mark5B using fuseMark5, which allows to mount the Mark5B disk packs as an external disk. Eight scans were scheduled to allow for different settings. Metsahövi recorded the data on two polarizations, while Yebes and Onsala only used one circular polarization. Since polarization sense was unknown at Yebes, 6 scans were recorded with the quarter wavelength plate between M6 and M7 in a given position and 2 were recorded after the plate was rotated 90 degrees.

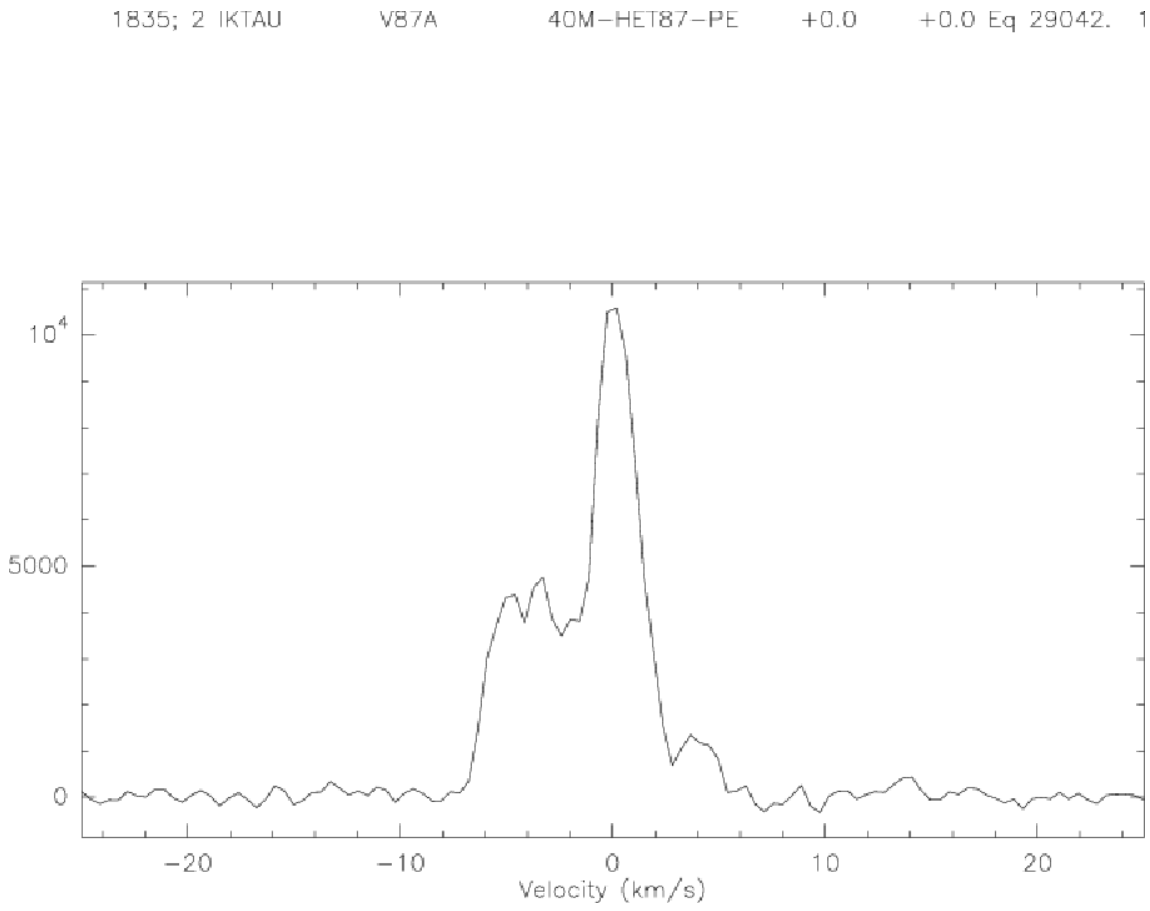

Figure 5: *SiO V1 (2-1) transition at 86243.430 MHz towards IK Tau with the 40 m. Spectral resolution is 125 KHz per channel. Amplitude calibration is incorrect.*

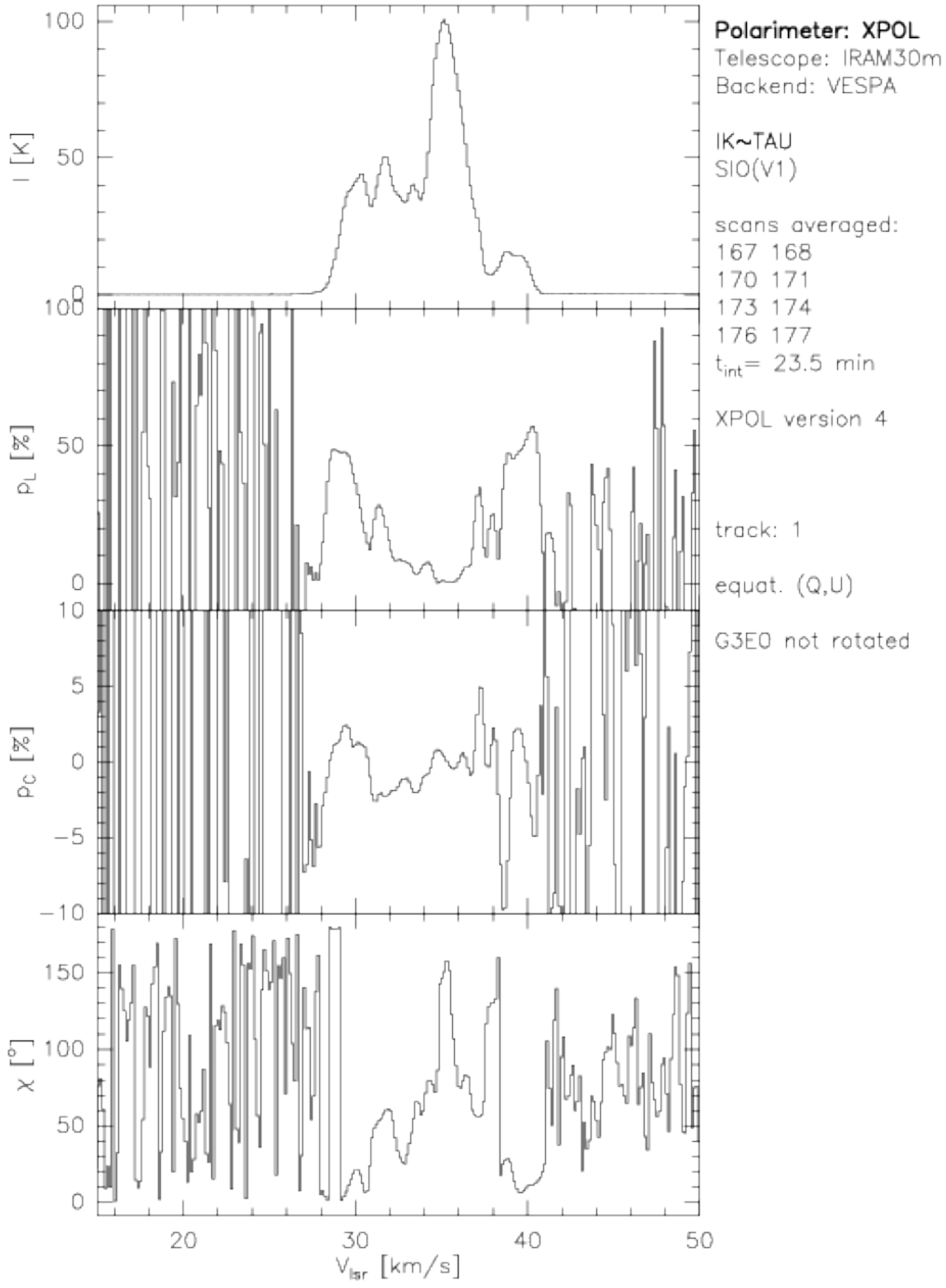

Figure 6: *SiO V1 (2-1) transition at 86243.430 MHz towards IK Tau with the 30 m. To obtain the flux in Janskys, the antenna temperature should be multiplied by 6*

Correlation was peformed by D. Graham and W. Alef at the correlator of MPI fuer Radioastronomie in Bonn.

Figs. 7 and 8 show the fringe plots obtained by the correlator between Onsala-Yebes and Metsahövi-Yebes. The signal towards 3C454.3 was integrated during 285 seconds. The phase of the correlated signal was below 1 radian for the whole 5 minute interval.

11 Conclusion

The results described here show that although observations with the 3 mm are possible, there is plenty of room for improvement and some works should be performed to increase the sensitivity of the system and produce data with aceptable quality.

A study to replace the membrane of the vertex by a new one made of a material with less loss, is ongoing. The replacement of the membrane is an important task that should be planned for next summer (2011) when the weather is milder and the probability of rain is low.

The surface of the main reflector should be adjusted according to results from holography observations. If the aperture efficiency increases, more sources will be detectable and it will be possible to create a pointing model that covers the whole sky. A new gain curve should be determined and focus effects depending on the environment temperature and solar insolation can be studied.

References

[Baars 2007] J. W. M. Baars. "The Paraboloidal Reflector Antenna in Radio Astronomy and Communication", Springer 2007.

[Cordobés 2009] D.Cordobés, J.A.López Pérez, C.Almendros, J.A.Abad, J.M.Yagüe, S.Henche "Diseño, montaje y medida de la unidad de FI del receptor de 3 mm", IT OAN 2009-4

[de Vicente 2010a] P. de Vicente, K. Matull, E. Sust, C. Albo. "Encoder hysteresis at the 40m radiotelescope". IT OAN-2010-2

[de Vicente 2010a] P. de Vicente. "Characterization of the 40m radiotelescope at 5, 6, 8 and 22 GHz", IT OAN 2010-10

[Malo 2010] I. Malo, J. D. Gallego, M. Diez, I. López, R. García, "Medida de la Permitividad a temperaturas criogénica y ambiente con el método de Perturbación de Cavidad", IT OAN 2010-09

[Tercero & Finn 2010] F. Tercero & T. Finn "Private communication"

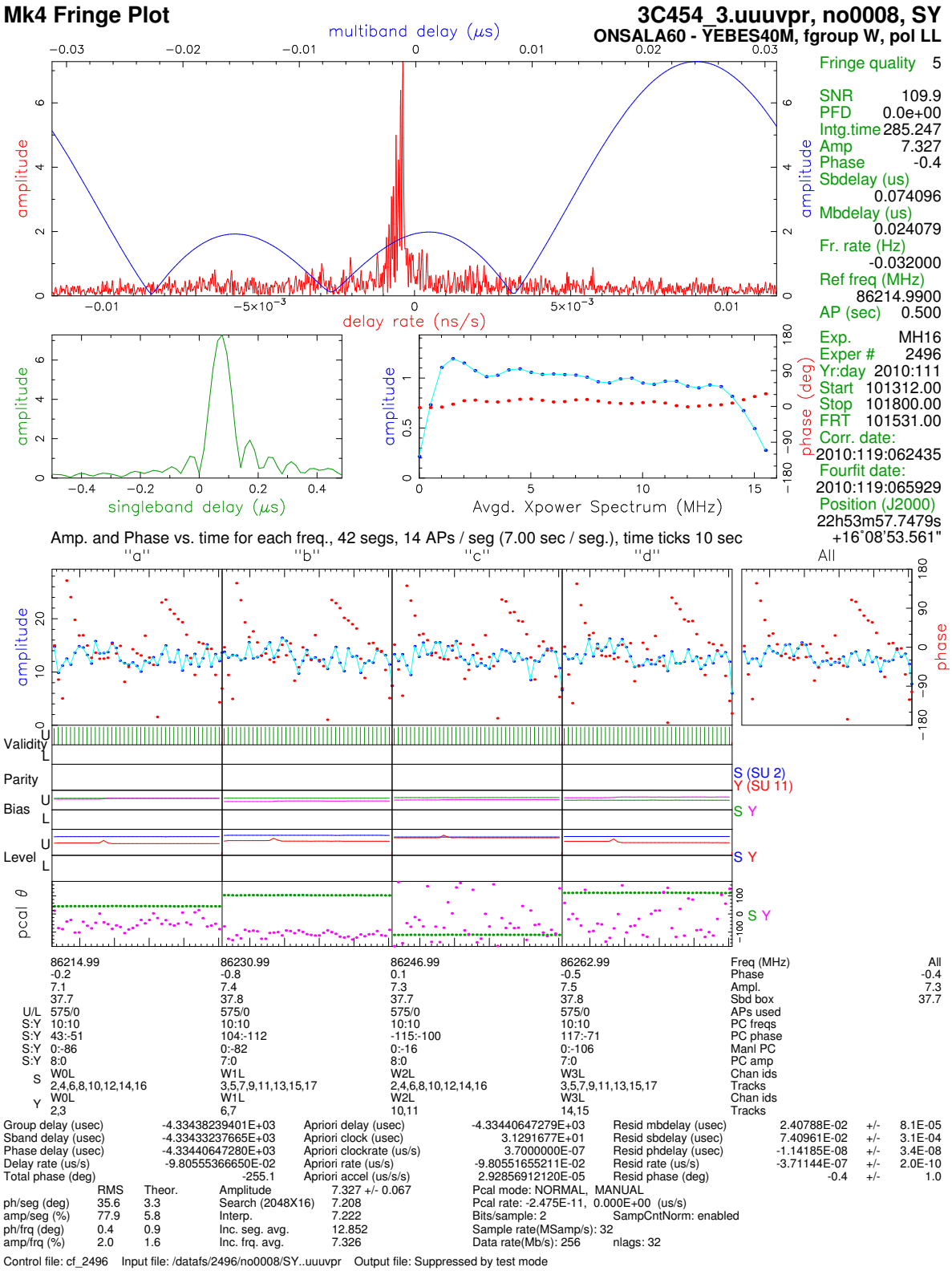

Figure 7: *Fringe plot obtained towards 3C454.3 between Onsala and Yebes.*

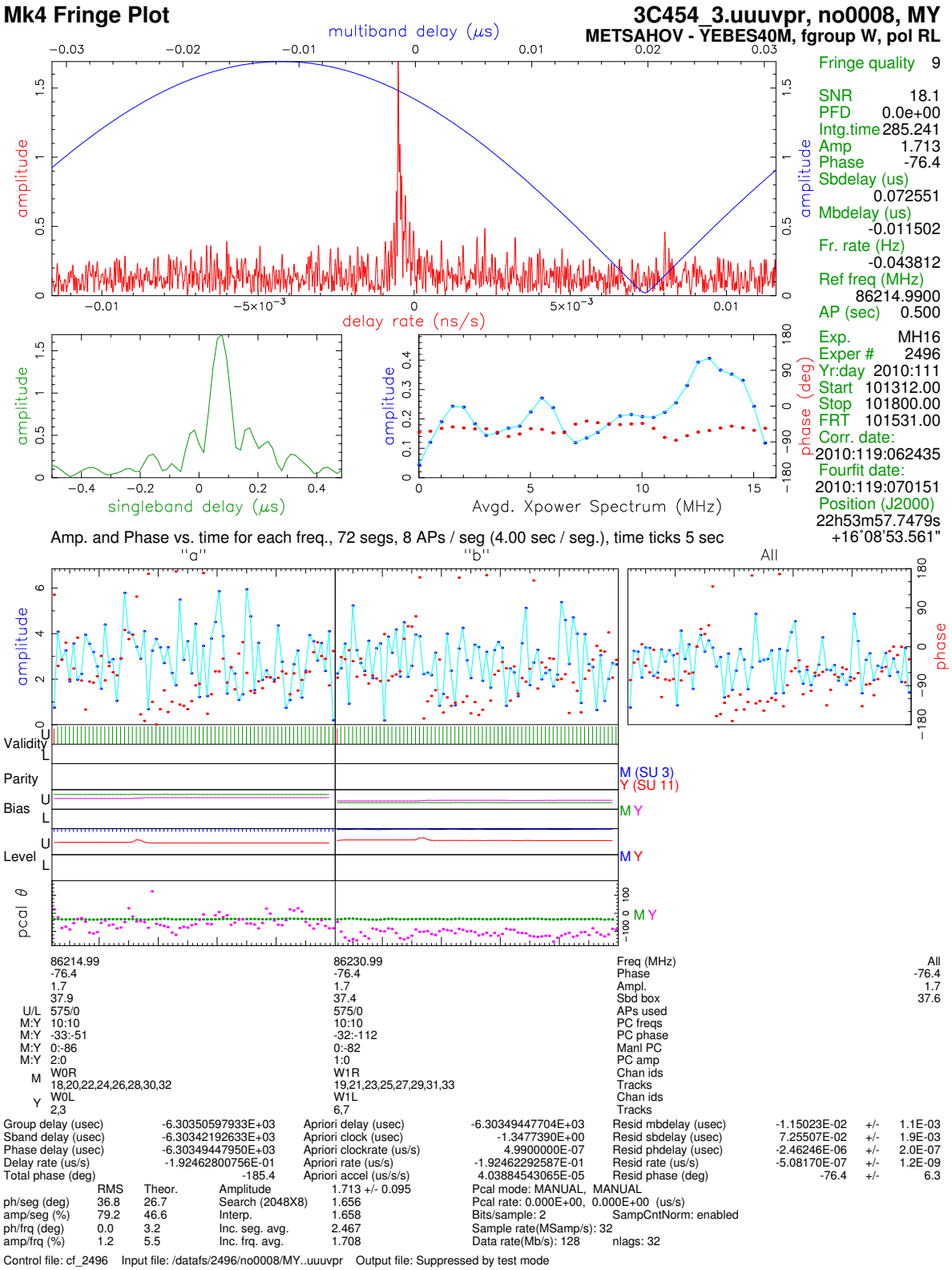

Figure 8: *Fringe plot obtained towards 3C454.3 between Onsala and Yebes.*